Energy and Buildings 42 (2010) 455–460

Contents lists available at ScienceDirect

Energy and Buildings

journal homepage: www.elsevier.com/locate/enbuild

Impacts of the shading-type building-integrated photovoltaic claddings on electricity generation and cooling load component through shaded windows

L.L. Sun *, H.X. Yang

Renewable Energy Research Group (RERG), Department of Building Services Engineering, The Hong Kong Polytechnic University, Kowloon, Hong Kong, China

ARTICLE INFO

Article history:
Received 8 October 2009
Accepted 8 October 2009

Keywords:
Shading-type building-integrated photovoltaic claddings
Electricity generation
Cooling load
Shaded window

ABSTRACT

The shading-type building-integrated photovoltaic (BIPV) claddings can act as power generators as well as external shading devices of a building, which reduce the energy consumption of the building. However, there is little information about energy impacts of different tilt angles of the shading-type BIPV claddings. By considering the typical meteorological conditions of Hong Kong, the energy performance of the shading-type BIPV claddings, in terms of the electricity generation and the cooling load reduction, is analyzed in this paper. The optimum tilt angle of PV modules for maximum electricity generation is found to be 20° instead of local latitude. Combining electricity generation and cooling load reduction, it can be concluded that the optimum tilt angles for the first type of the shading-type BIPV claddings vary from 30° to 50°, while the optimum tilt angle for the second type is 0°.

1. Introduction

According to the Hong Kong Annual Report of 2008 [1], buildings took up 89% of total electricity consumption in Hong Kong. Reducing electricity consumption in buildings is the ultimate goal to make buildings environment-friendly. Policy makers and developers have initiating energy conservation strategies for buildings. One of the most effective approaches is the application of the building-integrated photovoltaic (BIPV) modules. The PV modules integrated into building envelops can be used as curtain walls, windows, roofs and external shading claddings [2]. There are many reports about the researches and developments of BIPV walls [3,4], BIPV roofs [5,6] and BIPV windows [7,8]. There is little information about the shading-type BIPV claddings, though there have been many successful shading-type BIPV cladding systems around the world [9–11]. Yooa [12] evaluates the annual efficiencies of a shading-type BIPV cladding system and suggests that the shading-type BIPV claddings should be applied for both generating electricity and providing shading for the building.

In general, the shading-type BIPV claddings are oriented at the position that can receive the most desirable solar energy to obtain the maximum electricity generation. At the same time, a great amount of solar heat entering the windows can be prevented and the cooling load of the building can be reduced by the shading effect of the shading-type BIPV claddings. These benefits make buildings become more energy efficient. However, contradiction between the electricity generation and the cooling load reduction occurs. It is obvious that the PV modules produce the greatest shading effect when they are placed horizontally. However, this position is not the best for PV modules to obtain the most desirable electricity generation. It is difficult for engineers to select the optimum tilt angle of PV modules for a particular building. Thus, it is worth studying the impact of different tilt angles of PV modules on the energy saving in order to maximize the saving. This paper aims to find out the optimum tilt angles of the shading-type BIPV claddings for providing the most desirable energy saving effect in terms of electricity generation and cooling load reduction and to illustrate these results graphically for references of engineers or designers.

2. Modelling of the solar radiation on a tilt surface

For a tilt surface, the total solar radiation (G_{tt}) consists of the beam solar radiation (G_{bt}), the diffuse solar radiation (G_{dt}) and the ground reflected solar radiation (G_{rt}).

The beam part G_{bt} can be simulated by

$$G_{bt} = G_{bh} \cdot \frac{\cos\theta_t}{\cos\theta_h} = G_{bh} \cdot R_b \quad (1)$$

The equations from Duffie [13] are used for calculating the incidence angle of the beam solar radiation.

The ground reflected part G_{rt} can be simulated by

$$G_{rt} = G_{th} \cdot \rho \cdot \frac{1-\cos\beta}{2} \quad (2)$$

* Corresponding author.
E-mail address: 07901289r@polyu.edu.hk (L.L. Sun).

0378-7788/$ – see front matter © 2009 Elsevier B.V. All rights reserved.
doi:10.1016/j.enbuild.2009.10.014

If there is snow on the ground, the range of ρ is from 0.35 to 0.6. If there is no snow on the ground, ρ is about 0.2, which is a nominal value for green vegetation and some soil types.

The Perez model [14] is used for the diffuse solar radiation on a tilt surface:

$$G_{dt} = G_{dh} \cdot \cos^2\left(\frac{\beta}{2}\right) \cdot (1 - F_1) + G_{dh} \cdot F_1 \cdot \left(\frac{f_1}{f_2}\right) + G_{dh} \cdot F_2 \cdot \sin(\beta) \tag{3}$$

$$F_1 = F_{11}(\varepsilon) + F_{12}(\varepsilon) \cdot \Delta + F_{13}(\varepsilon) \cdot \theta_h \tag{4}$$

$$F_2 = F_{21}(\varepsilon) + F_{22}(\varepsilon) \cdot \Delta + F_{23}(\varepsilon) \cdot \theta_h \tag{5}$$

$$\varepsilon = \frac{(G_{bh}/\cos\theta_h + G_{dh})/G_{dh} + 1.041 \cdot \theta_h^3}{1.041 \cdot \theta_h^3} \tag{6}$$

$$\Delta = \frac{G_{dh}}{G_o} = \frac{G_{dh}}{1353 \cdot [1 + 0.033 \cdot \cos(360n/365)] \cdot \cos\theta_h} \tag{7}$$

The ratio f_1/f_2 determines the angular location of the circumsolar region and can be expressed as

$$\frac{f_1}{f_2} = \frac{\max[0, \cos\theta_t]}{\max[\cos 85, \cos\theta_h]} \tag{8}$$

For above models, G_{bh} and G_{dh} are necessitated. As the Hong Kong Observatory only offers the value of G_{th}, suitable models for dividing the total solar radiation into the beam and diffuse part are required. Li and Lam [15] analyzed the measured solar radiation and developed the correlation between the hourly diffuse ratio (G_{bh}/G_{th}) and sky clearness (ε) for Hong Kong. This model reflects the trend of more clouds and less frequent clear skies in Hong Kong, which is used in this paper. The weather data of the year 1989 are used for hourly simulation as discussed by Lu and Yang [16].

3. Modelling of electricity generation of PV modules

The performance of crystalline silicon PV modules depends on the physical variables of the solar cell material, the temperature of solar cell and the solar radiation exposed on the solar cell. One simplified applicable model developed by Lu and Yang [17] for the maximum power output of PV modules is used in this paper. The model and regressed parameters are described as follows:

$$P_m(t) = -(a_1 \cdot G_{tt}(t) + a_2) \cdot (T_a(t) + 0.03375 \cdot G_{tt}(t)) + a_3 \cdot G_{tt}(t) + a_4 \tag{9}$$

where the value of a_1, a_2, a_3, and a_4 utilized in the simulation is 0.0002, 0.0004, 0.1007 and 0.1018, respectively.

4. Modelling of cooling load of shaded window

4.1. Solar radiation absorbed by shaded window

The most significant effect of the overhang is to intercept the beam solar radiation from the sun before it reaches the window. The ratio of beam solar radiation received by a partly shaded window to that received by an unshaded window, F_u, can be defined as

$$F_u = \frac{A_u}{A_w} \tag{10}$$

The area-average solar radiation absorbed by the shaded window can be expressed by

$$G_w = G_{bw} \cdot F_u + G_{dw} \cdot F_{r\text{-}s} + G_{rw} \tag{11}$$

where $F_{r\text{-}s}$ is determined by the geometry and relative position of the window and the overhang [18].

4.2. Unshaded ratio determination

The value of F_u at any time not only depends on the dimensions of the overhang and the window but also on the incidence angle of the beam solar radiation entering through the window. In order to calculate the value of F_u, the shadow of the overhang projected on the window should be determined first. In the orthogonal coordinates (as shown in Fig. 1), *X*, *Y*, *Z* represents the direction of south, east and solar zenith, respectively. The parallelogram *OMCD* represents the window and the parallelogram *ABCD* presents the overhang.

At a particular moment, the position of the Sun can be determined by the zenith angle (θ_h) and the surface-solar azimuth angle (γ), so that the unit vector of the Sun, $\overline{V_s}$, can be expressed as

$$\overline{V_s} = [\sin\theta_h \cdot \cos\gamma, -\sin\theta_h \cdot \sin\gamma, \cos\theta_h]^T \tag{12}$$

As shown in Fig. 1, the vector $\overline{OA}$ can be presented as $[L_o, 0, H_w]^T$. Supposing that the projection of point *A* on the window is at point *A*′, the vector $\overline{OA'}$ can be found by employing the vector algebra law

$$\overline{OA'} = \overline{OA} + \lambda \cdot \overline{V_s} \tag{13}$$

where λ is a constant and can be written as

$$\lambda = -\frac{L_o}{\sin\theta_h \cos\gamma} \tag{14}$$

Thus, the vector $\overline{OA'}$ can be expressed as

$$\overline{OA'} = \left[0, L_o \tan\gamma, H_w - \frac{L_o}{\tan\theta_h \cos\gamma}\right] \tag{15}$$

If the position of point *A*′ can be determined, the area of quadrilateral *A*′*NCD* can be calculated. Therefore, the value of F_u can be obtained.

4.3. Solar heat gain absorbed by shaded window

The amount of solar heat gain entering through a window is usually determined in terms of solar heat gain factors (SHGF). In this paper, applicable models proposed by Powell [19] are used to calculate the value of SHGF and can be described as

$$SHGF_{bw} = G_{bw} \cdot F_u \cdot (\tau_b + \alpha_b \cdot N_i) \tag{16}$$

$$SHGF_{dw} = (G_{dw} \cdot F_{r-s} + G_{rw}) \cdot (\tau_d + \alpha_d \cdot N_i) \tag{17}$$

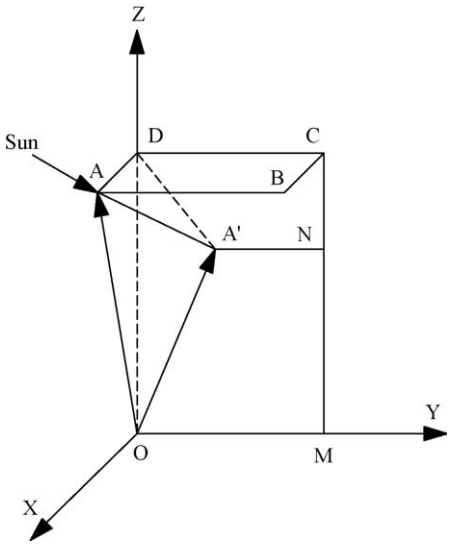

Fig. 1. The orthogonal coordinates.

$$N_i = \frac{h_i}{h_i + h_o} \tag{18}$$

The value of h_i used in the simulation is 8.29 W/(m^2 K), recommended by ASHRAE Hand Book [20]. The value of h_o depends on the speed and direction of the wind blowing over the widow. The models developed by Loveday and Taki [21] are used as follows:

$$h_o = 16.21 \cdot v_w^{0.452} \tag{19}$$

$$v_w = 0.68 \cdot v_o - 0.5(20^\circ \le \varphi \le 160^\circ) \tag{20}$$

$$v_w = 0.157 \cdot v_o - 0.027(\varphi < 20^\circ \text{ or } \varphi > 160^\circ) \tag{21}$$

The transmittance and absorptance for the beam component depends on the incidence angle of the beam solar radiation. The correlations developed by Stephenson [22] are used as follows:

$$\tau_b = -0.00885 + 2.71235\cos\theta_w - 0.62062\cos^2\theta_w - 7.07329\cos^3\theta_w + 9.75995\cos^4\theta_w - 3.89922\cos^5\theta_w \tag{22}$$

$$\alpha_b = 0.001154 + 0.77674\cos\theta_w - 3.94657\cos^2\theta_w + 8.57881\cos^3\theta_w - 8.38135\cos^4\theta_w + 3.01188\cos^5\theta_w \tag{23}$$

For the diffuse solar radiation and ground reflected solar radiation, the value of τ_d and α_d used in the simulation is 0.799 and 0.0544, respectively [22].

4.4. Cooling load calculation

The radiant time series (RTS) method [20] is a new simplified method for performing cooling load calculations that is derived from the heat balance method. The RTS method is developed in response to the desire to offer a method that is rigorous, yet does not require iterative calculations, and quantifies each component contribution to the total cooling load.

In the RTS method, the hourly cooling load of a window produced by the beam and diffuse solar heat gain can be expressed as

$$Q_{dw}(t) = r_{dw} \cdot \sum_{i=0}^{23} SHGF_{dw}(t-i) \cdot q_i + c_{dw} \cdot \sum_{i=0}^{23} SHGF_{dw}(t-i) \tag{24}$$

$$Q_{bw}(t) = r_{bw} \cdot \sum_{i=0}^{23} SHGF_{bw}(t-i) \cdot p_i + c_{bw} \cdot \sum_{i=0}^{23} SHGF_{bw}(t-i) \tag{25}$$

The value of r_{bw}, r_{dw}, c_{bw}, c_{dw}, p_i and q_i can be determined according to ASHARE Hand Book [20] when the window is selected.

5. Simulation prerequisites

5.1. Descriptions of the simulated window

The aim of this simulation is not only to investigate the optimum power generation of PV modules, but also to find out the effects of the shading-type BIPV claddings on the cooling load reduction of a window. The dimensions of the selected window are 4.5 m × 1.5 m, as shown in Fig. 2. PV modules can be integrated into the vertical walls below and above the windows. The width of the PV modules is as the same as that of the windows. In Hong Kong, the south facade can receive the maximum annual solar radiation. So the PV modules installed on the south facade can generate the maximum annual electricity. On the other hand, the shading effect of the overhangs is the most significant when they are installed above the south windows. Thus, the energy effects of shading-type BIPV claddings installed on the south facade are discussed in this paper only.

5.2. Structures of shading-type BIPV claddings

In this paper, the energy effect of the shading-type BIPV claddings with different tilt angles is analyzed. Two types of shading-types BIPV claddings are proposed to analyze the electricity generation and cooling load reduction. Fig. 3 shows the schematic of these two shading-type BIPV cladding structures.

(1) *Structure A*: The height of the wall between windows of two consecutive floors is fixed. In this arrangement, the length of PV modules varies as tilt angle changes, so as to the area of PV modules.
(2) *Structure B*: The length of PV modules is fixed. Since the width of PV modules is as same as that of the windows, the area of PV modules is also fixed.

6. Simulation results and discussions

6.1. Annual electricity generation of PV modules

Ten tilt angles, from 0° to 90°, were used for calculating the annual electricity generation of the PV modules, as shown in Fig. 4. In general, PV modules produce more electricity annually at smaller tilt angles than larger ones. When the tilt angles are larger than 40°, the annual electricity generation drops quite signifi-

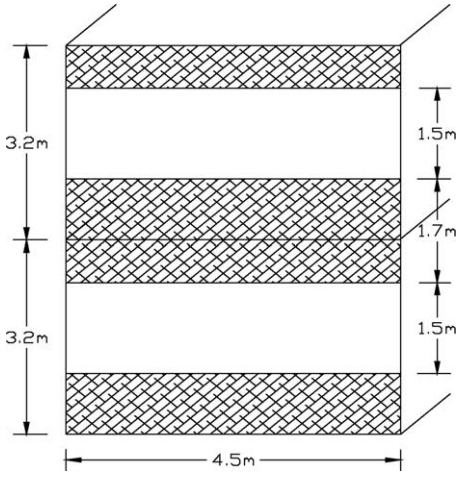

Fig. 2. The schematic of the widow.

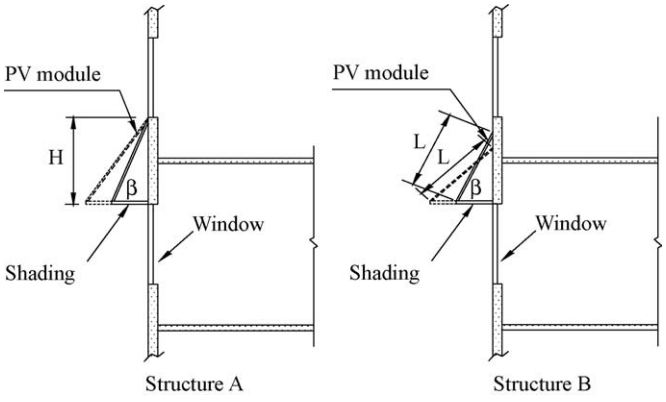

Fig. 3. The schematic of the shading-type BIPV claddings.

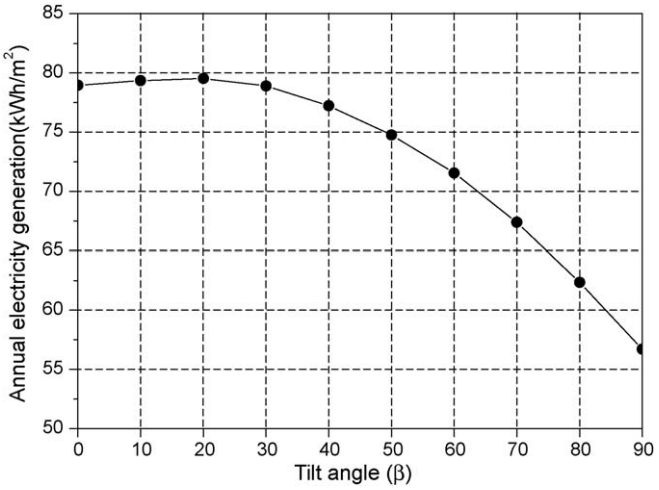

Fig. 4. Effect of tilt angle on annual electricity generation.

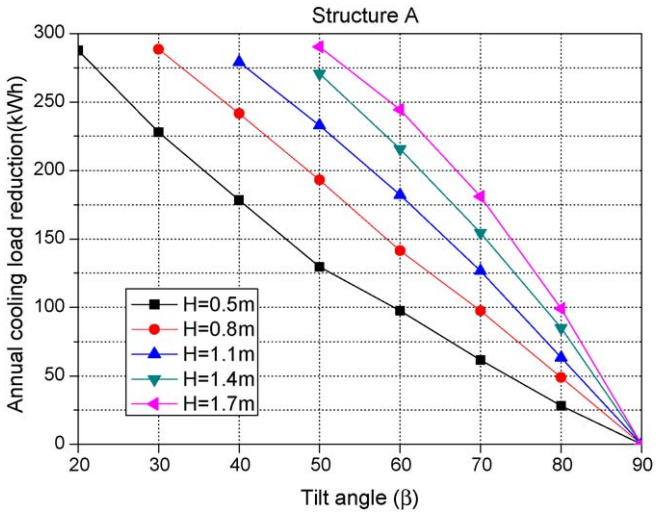

Fig. 5. Annual cooling load reduction of structure A.

cantly. When the tilt angle equals 20°, the maximum annual electricity generation of 79.55 kWh/m^2 can be obtained. The minimum annual electricity production is 57.02 kWh/m^2 when the tilt angle is 90°.

It can be seen from Fig. 4 that the optimum tilt angle of the PV modules in terms of annual electricity generation is 20°, rather than 22.3°, the latitude of Hong Kong. This result is different from the notion that in general, the optimum tilt angle equals the local latitude. The main reasons for this deviation are related to the meteorological conditions of Hong Kong.

6.2. Annual cooling load reduction

In both two structures of the shading-type BIPV claddings described above, the length of the overhang depends on the tilt angle of PV modules when H or L is fixed. A maximum length of 1.5 m for the overhang is used in this simulation because this is the maximum projection from an external wall that can be exempted from the Gross Floor Area and Site Coverage calculation [23]. On the other hand, it is difficult to install if the overhang is too long. Thus different tilt angles were selected for different conditions so that the length of the overhang is smaller than 1.5 m.

6.2.1. Structure A

The heights of the opaque wall (H) chosen to be simulated are 0.5, 0.8, 1.1, 1.4 and 1.7 m. Different tilt angles were selected for different H values to ensure that the length of the overhang is smaller than 1.5 m. Fig. 5 illustrates the simulation results of the annual cooling load reduction for this structure. It can be observed that for each H, the annual cooling load reduction decreases as the tilt angle increases. The reason is that when the tilt angle increases, the length of the overhang decreases. The annual cooling load reduction decreases to zero when the tilt angle increases to 90°. So the PV modules should be installed at smaller tilt angles in terms of obtaining the maximum cooling load reduction.

6.2.2. Structure B

For structure B, the length of PV modules (L) is fixed. The lengths of PV modules chosen to be simulated are 0.3, 0.6, 0.9, 1.2 and 1.5 m. The annual cooling load reductions are simulated at ten tilt angles from 0° to 90° for each length. Fig. 6 shows the simulation results. The amount of annual cooling load reduction decreases as the tilt angle of the PV modules increases or the length of PV modules decreases. The annual cooling load reduction drops quickly when the tilt angles are larger than 30°. When the length of the PV modules is longer than 0.9 m, when L becomes larger, the cooling load reduction increases insignificantly. So the best position of PV modules is in horizontal when only the annual cooling load reduction is considered.

6.3. Combined effects of electricity generation and cooling load reduction

As mentioned above, the annual electricity generation and the annual cooling load reduction produced by the shading-type BIPV claddings will contribute to the electricity saving of buildings at the same time. It is necessary to analyze the combined effects of these two contributions and to evaluate the optimum position of the shading-type BIPV claddings so that the maximum electricity saving is achieved. Firstly, the annual cooling load reduction should be converted into the electricity consumption reduction. By using the COP of the HVAC system, the annual cooling load reduction can be converted into annual electricity consumption reduction. Supposing that the building is cooled by an air cooled HVAC system, the value of COP is set to be 2.8 [24]. Thus, the

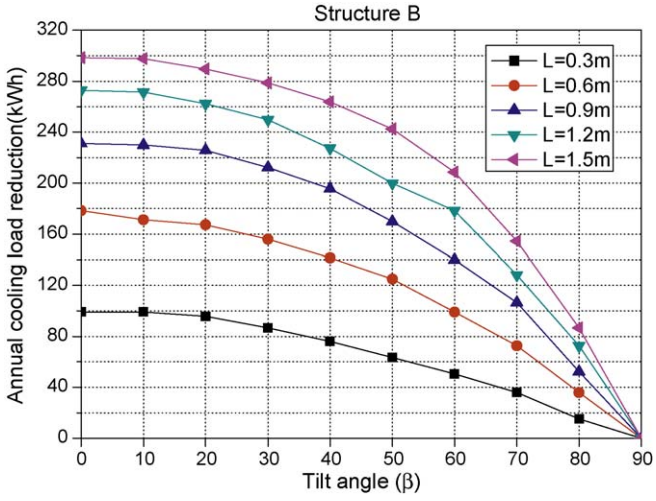

Fig. 6. Annual cooling load reduction of structure B.

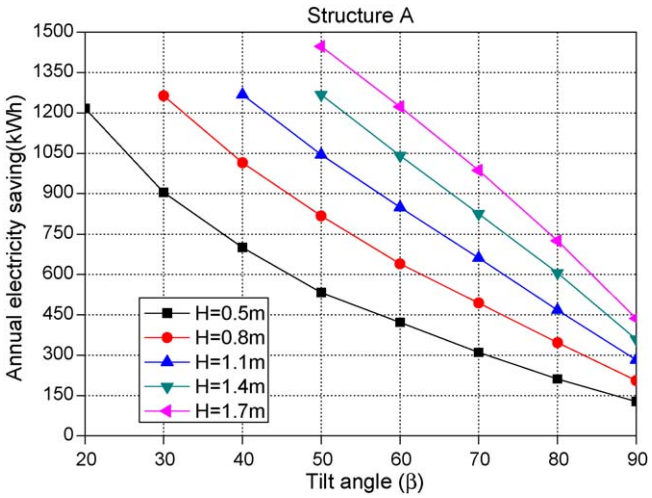

Fig. 7. Annual electricity saving of structure A.

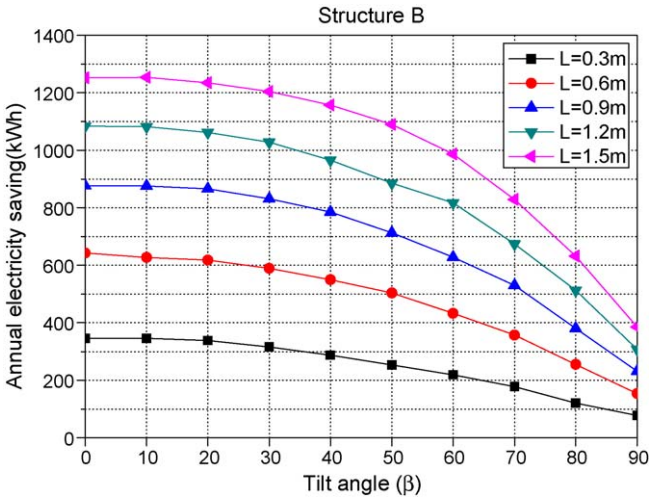

Fig. 9. Annual electricity saving of the structure B.

combined effects can be analyzed for the following two types of the shading-type BIPV claddings.

6.3.1. Structure A

For structure A, five values of the height *H* mentioned above were chosen in this simulation. These simulation results are shown in Figs. 7 and 8. It can be shown from Fig. 7 that the annual electricity saving increases when the tilt angle decreases or when the value of *H* increases. The reason is that both the annual electricity generation and the annual cooling load reduction increases in these two situations. Fig. 8 shows that with the same value of *H*, the maximum annual electricity saving per unit PV module area does not occur at the smallest tilt angle. These optimum tilt angles are different for different values of *H*. Table 1 summarize these optimum tilt angles of the structure A for various heights.

6.3.2. Structure B

For the structure B, the length of PV modules is fixed. Five lengths of PV modules were used in this simulation, as mentioned above. The simulation results are shown in Figs. 9 and 10. As the tilt angle increases from 0° to 90°, both the annual electricity saving and annual electricity saving per unit PV area decrease. The shading-type BIPV claddings can produce the greatest energy saving effect when the tilt angle equal 0°. It can be also found that although the annual electricity saving is greater when using longer

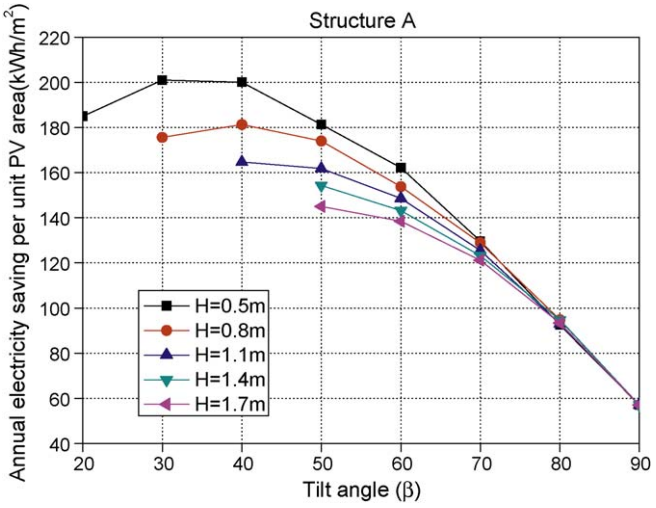

Fig. 8. Annual electricity saving per unit PV area of structure A.

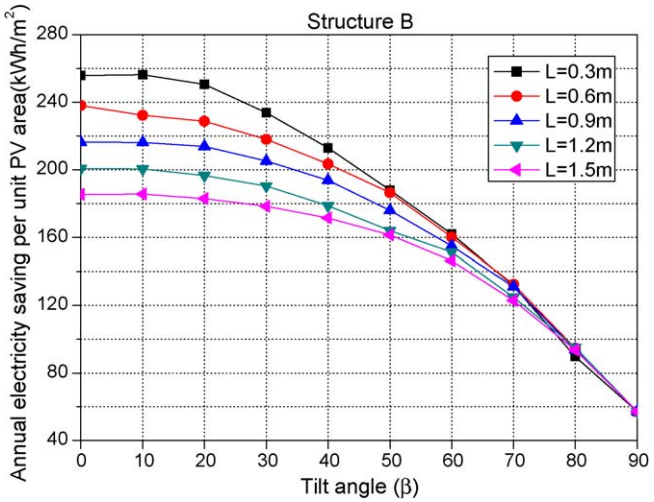

Fig. 10. Annual electricity saving per unit PV area of the structure B.

Table 1
Summary of optimum tilt angles for structure A.

H	0.5 m	0.8 m	1.1 m	1.4 m	1.7 m
Optimum tilt angle	30°	40°	40°	50°	50°

PV modules, the amount of annual electricity saving per PV unit area of shorter PV modules is larger. Since the cost of shorter PV modules is lower than that of longer ones, it concludes that the installation of short PV modules is more cost-effective for building facade areas between windows of a building.

7. Conclusions

The impact of the tilt angles on the energy performance of the shading-type BIPV claddings is analyzed in this paper in terms of annual electricity generation and annual cooling load reduction for a building. It concludes that the shading-type BIPV claddings on south facade can produce more electricity annually at the tilt angle of 20°, which is not equal to the local latitude of Hong Kong. The main reason is that the meteorological conditions of Hong Kong have also been considered in this simulation. Since the actual meteorological data are used in this paper, the results are practical and realistic.

The energy performance of two types of the shading-type BIPV claddings have been analyzed and discussed separately. For

structure A, different optimum tilt angles of the shading-type BIPV claddings are obtained for different cladding heights. In general, the optimum tilt angles for different heights vary from 30° to 50°. When using a smaller height, the annual electricity saving per unit PV area is greater. For the structure B, the shading-type BIPV claddings produce the greatest energy saving effect when they are installed horizontally. When the areas of PV modules are considered, it can be found that shorter PV modules would produce more energy saving effect per unit area and be more cost-effective than longer ones.

Nomenclature

G_{tt}	total solar radiation on a tilt surface (W/m^2)
G_{th}	total solar radiation on a horizontal surface (W/m^2)
G_o	extraterrestrial solar radiation on a horizontal surface (W/m^2)
R_b	geometric factor
f_1,f_2	brightness coefficient
F_{11},F_{12},F_{13},F_{21},F_{22},F_{23}	Ferez model coefficient
n	day of a year
A_u	area of the unshaded window (m^2)
A_w	area of the whole window (m^2)
$F_{r\text{-}s}$	review factor from sky
L_o	length of overhang (m)
H_w	height of window (m)
T_a	air temperature (K)
SHGF	solar heat gain factor (kWh/m^2)
N_i	inward-flowing fraction of absorbed solar radiation
h_i,h_o	heat transfer coefficient of inside and outside surface (W/(m^2 K))
v_w	wind speed outside of window (m/s)
v_o	wind speed from observatory (m/s)
r,c,p,q	RTS coefficient

Greek letters

θ	incidence angle of beam solar radiation (°)
β	tilt angle (°)
ρ	ground reflectance
ε	sky clearness
Δ	sky brightness
γ	surface-solar azimuth angle (°)
τ	transmittance
α	absorptance
φ	incidence angle of wind (°)

Indices

b	beam part
d	diffuse part
r	ground reflected part
t	tilt surface
h	horizontal surface
w	window

Acknowledgement

The work described in this paper was supported by a grant from the Guangdong - Hong Kong Technology Cooperation Funding Scheme (TCFS).

References

[1] The Information Services Department of Hong Kong SAR Government, The Hong Kong annual report of 2008, 2008.
[2] J. Benemann, O. Chehab, E.S. Gabriel, Building-integrated PV modules, Solar Energy Materials & Solar Cells 67 (2001) 345–354.
[3] H.X. Yang, J. Burnett, J. Ji, Simple approach to cooling load component calculation through PV walls, Energy and Buildings 31 (3) (2000) 285–290.
[4] J. Ji, H. Yang, W. He, G. Pang, J.P. Liang, B. Bin, Modeling of a novel Trombe wall with PV cells, Building and Environment 42 (2007) 1544–1552.
[5] L. Mei, D.G. Infield, R. Gottschalg, D.L. Loverday, D. Davies, M. Berry, Equilibrium thermal characteristics of a building integrated photovoltaic tiled roof, Solar Energy 83 (2009) 1893–1901.
[6] S. Ubertini, U. Desideri, Performance estimation and experimental measurements of a photovoltaic roof, Renewable Energy 28 (2003) 1833–1850.
[7] Y.Y. Fung, H.X. Yang, Study on thermal performance of semi-transparent building-integrated photovoltaic glazings, Energy and Buildings 40 (3) (2008) 341–350.
[8] J. Han, L. Lu, H.X. Yang, Thermal behaviour of a novel type see-through glazing system with integrated PV cells, Building and Environment 44 (2009) 2129–2136.
[9] J. Ohno, Examples of Successful Architectural Integration of PV: Japan, Progress in Photovoltaics: Research and Application 12 (2004) 471–476.
[10] D. Prasad, M. Snow, Examples of successful architectural integration of PV: Japan, Progress in Photovoltaics: Research and Application 12 (2004) 477–483.
[11] I.B. Hagemann, Examples of successful architectural integration of PV: Germany, Progress in Photovoltaics: Research and Application 12 (2004) 461–470.
[12] S.H. Yooa, E.T. Lee, Efficiency characteristic of building integrated photovoltaics as a shading device, Building and Environment 37 (2002) 615–623.
[13] J.A. Duffie, W.A. Beckman, Solar Engineering of Thermal Processes, John Wiley & Sons, 1980.
[14] R. Perez, P. Ineichen, R. Seals, Modelling of daylight availability and irradiance components from direct and global irradiance, Solar Energy 44 (1990) 271–289.
[15] D.H.W. Li, J.C. Lam, Analysis of solar heat factors using sky clearance index and energy implications, Energy Conversion and Management 42 (2001) 555–571.
[16] L. Lu, H.X. Yang, Study on typical meteorological years and their effect on building energy and renewable energy simulations, ASHARE Transaction 110 (2) (2004) 424–431.
[17] L. Lu, H.X. Yang, A study on simulations of the power output and practical models for building integrated photovoltaic systems, Journal of Solar Energy Engineering 126 (2004) 929–935.
[18] D.M. Utzinger, S.A. Klein, A method of estimating monthly average solar radiation on shaded receivers, Solar Energy 23 (1979) 369–378.
[19] G.L. Powell, J.I. Yellott, Solar heat gain factors on average days, Proceeding of American Section of the International Solar Energy Society Annual Meeting (1980) 826–830.
[20] American Society of Heating, Refrigerating and Air Conditioning Engineering, ASHARE Handbook-Fundamentals, ASHARE Inc., 1997.
[21] D.L. Loveday, A.H. Taki, Convective heat transfer coefficients at a plane surface on a full-scale building façade, International Journal of Heat and Mass Transfer 39 (8) (1996) 1729–1742.
[22] D.G. Stephenson, Equations for solar heat gain through windows, Solar Energy 9 (2) (1965) 81–86.
[23] Hong Kong Building Department, Joint Practice Note No. 1—Incentives for Green Buildings, 2001.
[24] F.W.H. Yik, J. Burnett, I. Prescott, Predicting air-conditioning energy consumption of a group of buildings using different heat rejection methods, Energy and Buildings 33 (2001) 151–166.